COMMUNICATION

Diffusion-Controlled, Self-Organized Growth of Symmetric Wrinkling Patterns

By *Jun Young Chung, Adam J. Nolte,* and *Christopher M. Stafford**

Compressing a thin film on a compliant substrate can lead to the spontaneous formation of highly ordered patterns, a phenomenon known as surface wrinkling.[1–5] These self-organized patterns can occur in a variety of morphologies and spatial configurations due to differences in the applied stress state. A common natural example of this phenomenon is human skin,[3,4] which wrinkles perpendicular to the compressive stress direction when bunched together between two fingers. The same patch of skin, however, will display a spoke-like radial pattern when indented or pulled up at a localized point due to lateral contraction induced by the Poisson effect,[3] demonstrating that the wrinkles prefer to orient themselves perpendicular to the axis of principal compressive stress. Motivated by these observations, we investigate here the initiation, organization, and growth of surface wrinkling patterns in UV/ozone (UVO)-treated polymer films exposed to solvent vapor. In particular, we demonstrate that unique and previously unreported pattern symmetries are formed in response to in-plain stresses caused by localized diffusion of solvent into the film; furthermore, these patterns can be powerful morphological indicators of the kinetics of solvent diffusion within the film.

We focus on two distinct anisotropic patterns, namely *spokes* and *targets*. These patterns initially develop at random defect sites in the film, and expand until their growth is stopped by neighboring patterns or film boundaries (Fig. 1), analogous to crystallization and other growth processes involving ordering thermodynamic systems and chemical-reaction processes.[6] Our results suggest that the type of pattern and its speed of growth is coupled to the degree of UVO crosslinking, which in turn governs the rate of solvent diffusion into the film. Spoke and target patterns are associated with Fickian and Case II diffusion behavior, respectively,[7] as these kinetic regimes establish distinct stress fields that favor the formation of wrinkles in those specific morphologies. Moreover, we show that precise positional control and long-range ordering of the patterns can be achieved by producing predefined defects in the film. So far, the study of self-organization via wrinkling processes has largely focused on *static* structures, but this simple yet novel approach is ideally suited for studying the rich *dynamics* of wrinkling, which could facilitate a broader understanding of the wrinkling phenomenon. This approach could also serve as a test-bed for studying topography-driven phenomena (e.g., wettability[8,9] and adhesion[10]) and diffusion-related processes.[7]

A sketch of the experimental set-up is depicted in Figure 2a. The films used in this study were prepared by spin-casting a solution of polystyrene (PS) in toluene onto a clean silicon wafer. Film thicknesses on the order of hundreds of nanometers were used in order to constrain the system to a 2D diffusion geometry. The surface of the spin-cast film was treated with UVO for a controlled period of time, leading to oxidation and crosslinking of the PS chains in the near surface region.[11] The film was then placed into a closed chamber saturated with toluene vapor at room temperature. Upon exposure to the vapor, the internal osmotic pressure induced by the preferential swelling of the unmodified PS resulted in a net compressive stress in the system.[5,12] When the stress exceeded a critical threshold value,[9] surface wrinkles began to form with the pattern morphology exhibiting a clear dependence on the length of UVO exposure. A rich variety of patterns was observed by simply varying the exposure time between 2 and 40 min; these included flowerlike patterns, spokes, targets, labyrinths, and dots, as shown in Figure 2b. These patterns persisted for several weeks after removal of the samples from the solvent chamber, consistent with the notion that the polymer undergoes viscous flow during wrinkling, and is kinetically trapped in the wrinkled morphology when the PS returns to a glassy state.[1c,12a]

The characteristic wavelength of the observed patterns as determined from 2D Fast Fourier Transform (FFT) analysis of microscope images was roughly proportional to the UVO exposure time (t_{UVO}). This fact can be understood knowing that with longer exposure times, the bending stiffness (B_f) of the surface layer increases, due to a growth in both its Young's modulus (E_f; due to densification and crosslinking) and thickness (h_f), as $B_f \sim E_f h_f^3$. These changes in the layer have been qualitatively confirmed using X-ray reflectivity. The equilibrium wrinkling wavelength (λ) is expected to vary as $\lambda \sim h_f(E_f/E_s)^{1/3} \sim (B_f/E_s)^{1/3}$,[2,3] with E_s being the Young's modulus of the swollen PS underlayer. Thus, λ increases with t_{UVO} as shown in Figure 2c, similar to previous reports for poly(dimethylsiloxane) treated with oxygen plasma or UVO.[2,5]

We chose to focus on the details of the spatio–temporal ordering of two distinct anisotropic patterns (i.e., spokes and targets). Spoke patterns (Fig. 3a) were generally observed after relatively short UVO exposures ($t_{UVO} \approx 3$ min, under our experimental conditions). Atomic force microscopy (AFM) imaging revealed pattern features that were nanometers in height and micrometers in width. Although the wavelength (λ) as measured in the theta direction remained constant, the amplitude

[*] Dr. C. M. Stafford, Dr. J. Y. Chung, Dr. A. J. Nolte
Polymers Division
National Institute of Standards and Technology
100 Bureau Drive
Gaithersburg, MD 20899 (USA)
E-mail: chris.stafford@nist.gov

DOI: 10.1002/adma.200803209

WILEY InterScience® DISCOVER SOMETHING GREAT
© 2009 WILEY-VCH Verlag GmbH & Co. KGaA, Weinheim

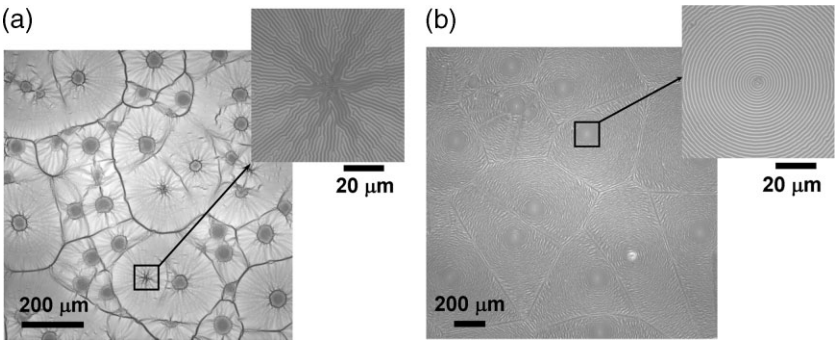

Figure 1. Optical microscopy images of wrinkling patterns formed in a 500 nm thick, UVO-treated polystyrene film exposed to toluene vapor. Patterned regions initiated from random surface defects, and grew until they collided and filled the film surface with a polycrystalline-like grain structure. The wrinkle morphology inside each grain is controlled by the UVO exposure time: a) spoke patterns ($t_{UVO} = 3$ min) and b) target patterns ($t_{UVO} = 5$ min).

(A) decayed as a function of radial distance (r) from the center of pattern (Fig. 3b). For moderately long UVO exposure times ($5 \text{ min} \leq t_{UVO} < 15$ min), we typically observed target patterns in which the wrinkle crests aligned in concentric rings with nearly constant spacing between the rings (λ) and uniform amplitude (A) throughout the entire pattern (Fig. 3c and d). In some rare cases, we observed outwardly rotating spiral patterns instead (not shown).

Close inspection of the films revealed that the formation and growth of both spoke and target patterns occurred at defects in the film surface – the patterns developed locally and spread over large areas (typical dimensions of several hundreds of micrometers; see Fig. 1), analogous to the self-organized growth observed in many physical, chemical, and biological systems.[6] Snapshots of the time evolution of the spoke and target patterns are presented in Figure 4.

In Figure 4a, the temporal growth of each pattern morphology is presented. The circular wrinkled front of the spoke pattern began forming only seconds after introduction to the solvent environment, and the radial growth rate went approximately as the square root of time (see inset plot), suggesting Fickian diffusion kinetics[7,13] (since the driving force for wrinkling growth is the osmotic stress due to solvent vapor diffusing into the glassy polymer, we consider the distance of the wrinkled front, R, to correspond roughly to the diffusion length). This type of behavior has been very recently observed for Ti/PS membranes under exposure to toluene vapor.[14] The target pattern, on the other hand, required an induction time (t_i) for pattern initiation on the order of minutes, and then grew radially with a linear time dependence (Fig. 4b). Thus, the appearance of target patterns in the samples subjected to longer t_{UVO} seems to suggest a Case II diffusion mechanism,[7] which is characterized by a linear advance of the solvent front; indeed, a transition from Fickian to Case II kinetics has been previously observed for glassy polymers in which diffusion is limited by the surface flux of the diffusing species.[15]

The above experimental observations suggest a mechanism for how both spoke and target patterns emerge. The formation of spokelike patterns was typically observed at a relatively short

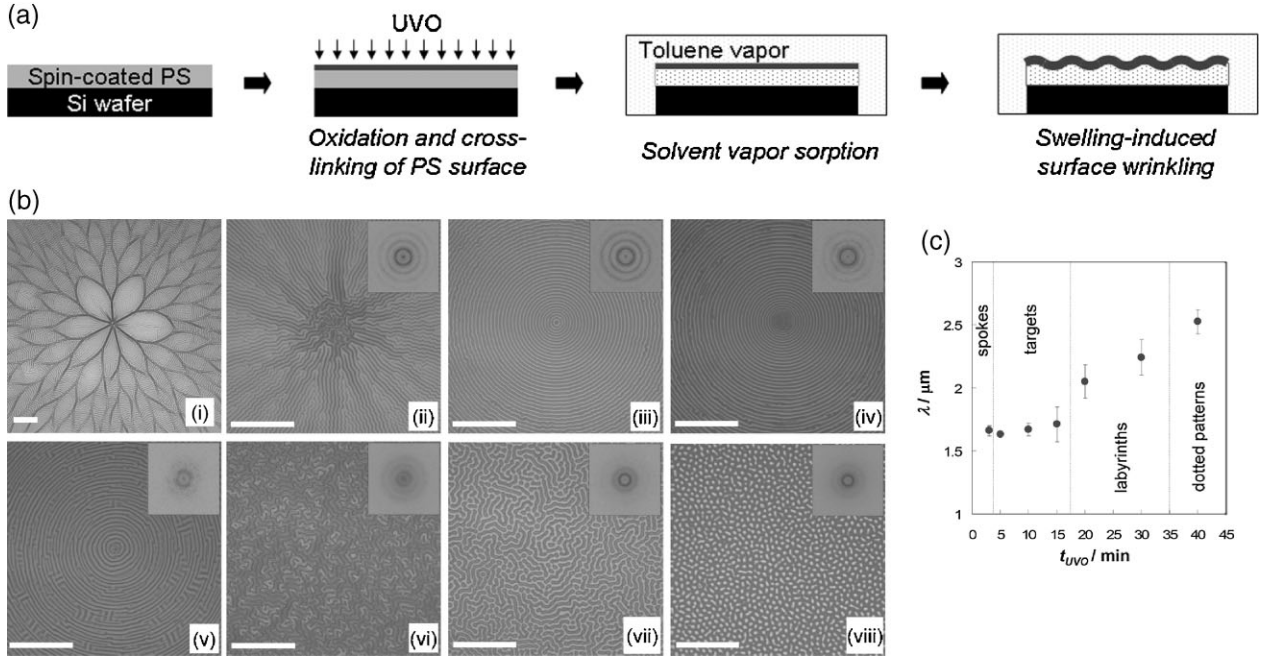

Figure 2. Variety of morphological patterns via swelling-induced surface wrinkling. a) Schematic of the experimental set-up for creating patterns using swelling-induced surface instabilities of UVO-treated polymer films. b) Optical microscopy images of various wrinkling patterns produced on 500 nm thick PS films with different UVO exposure times (t_{UVO}); i) 2, ii) 3, iii) 5, iv) 10, v) 15, vi) 20, vii) 30, and viii) 40 min. Scale bars = 30 μm. Insets display the results of 2D FFT analysis of microscope images, demonstrating a characteristic length scale (wavelength) for the surface undulations. c) Measured wavelength (λ) versus UVO exposure time (t_{UVO}). Dotted vertical lines indicate observed transitions in pattern morphology.

© 2009 WILEY-VCH Verlag GmbH & Co. KGaA, Weinheim

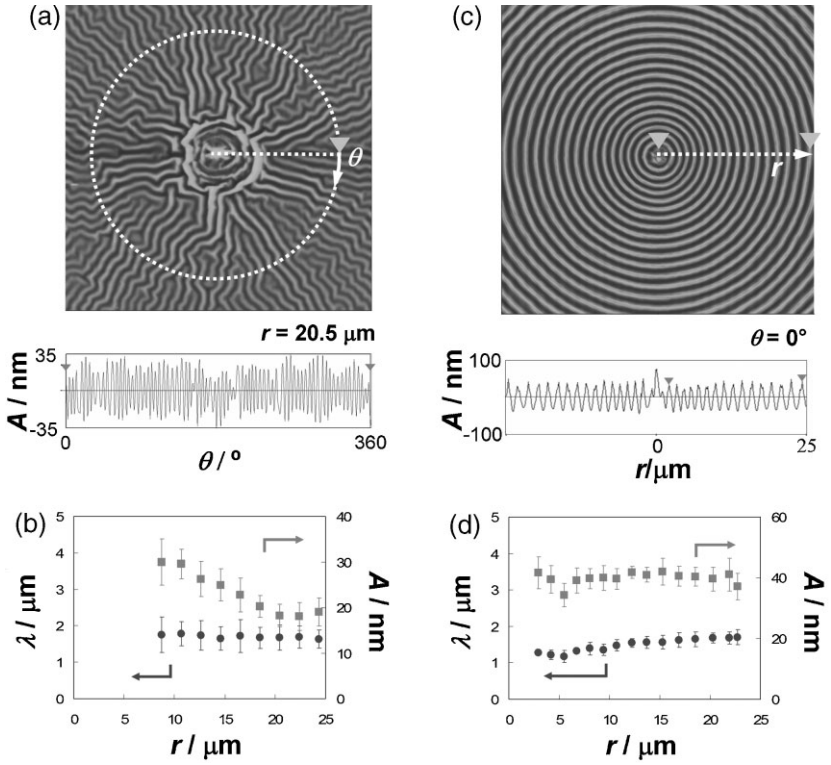

Figure 3. Formation of spoke and target patterns. a) AFM height image (50 μm × 50 μm) of the spoke pattern produced on a 500 nm thick PS film with $t_{UVO} = 3$ min. b) Azimuthally averaged wavelength (λ) and amplitude (A) as a function of radius (r). λ remains constant with r at 1.7 μm ± 0.05 μm, while A decreases as r increases. c) AFM height image (50 μm × 50 μm) of the target pattern comprising a series of concentric rings formed on a 500 nm thick PS film after $t_{UVO} = 5$ min. d) λ and A as a function of r. Both λ and A remain nearly constant at (1.5 ± 0.1) μm and (40 ± 2) nm, respectively.

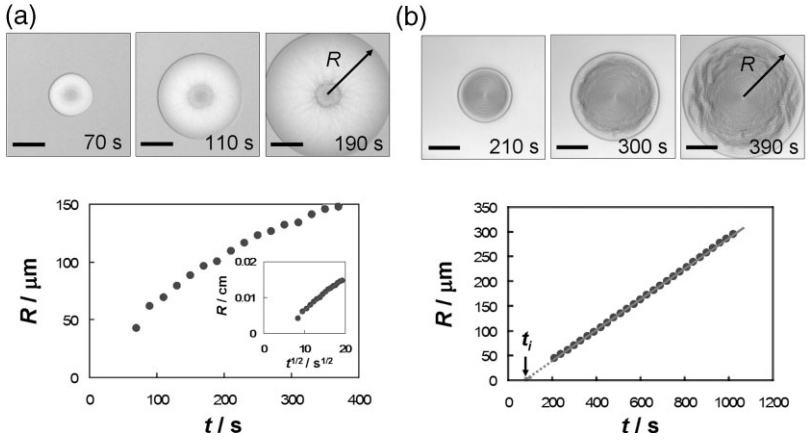

Figure 4. A sequence of snapshots of the time evolution of spoke and target patterns formed on a 500 nm thick PS film. These patterns initially nucleated at randomly distributed defect sites and then expanded to a size readily visible to the eye. a) $t_{UVO} = 3$ min. The plot shows radius of the wrinkled front (R) versus elapsed time (t). R was replotted against $t^{1/2}$ (inset) and fitted with a linear regression line, showing that the data collapse on a single line given by $R \approx 9.4 \times 10^{-4} t^{1/2}$. b) $t_{UVO} = 10$ min. The plot shows that R increases linearly with t, and the solid line is the best fit with $R = 0.32\ t - 23.6$. From the data, the growth velocity of target pattern was found to be $V \approx 0.3$ μm s^{-1}. The nonzero horizontal intercept corresponds to the induction time ($t_i \approx 80$ s) required for pattern initiation, the existence of which is known as a typical characteristic of Case II diffusion [7]. Scale bars = 30 μm.

t_{UVO}. We hypothesize that the presence of external impurities, such as dust particles, on the surface may serve as initiation sites, as suggested by a recent study of starburst defects in powder coatings.[16] As illustrated in Figure 5a, when a defect is present on the surface of the film, it will presumably serve as a locus of solvent vapor uptake and diffusion into the film. The swelling-induced stress in the film is expected to be highest near the solvent entry point and decrease along the radial direction due to diffusion. In addition, Poisson contraction due to some longitudinal (out-of-plane) swelling should orient the maximum stress direction in circular lines surrounding the surface defect[16] (Fig. 5a; see directional arrows in Fig. 5b). When the compressive stress exceeds the critical value, it induces wrinkling orthogonal to the direction of compressive stress, resulting in a spoke pattern whose boundary grows with the Fickian diffusion of solvent further into the film. This hypothesis, which assumes a radial decay of the compressive stress in the film, also explains the amplitude decay of the spoke-like wrinkles at increasing distances from the pattern center (Fig. 3b), as the wrinkling amplitude is known to increase with applied strain (or stress).[9,17]

In the case of a relatively long t_{UVO}, one would expect a greater resistance to diffusional penetration of the thick, crosslinked layer. Thus, the flux of solvent into the film becomes the limiting kinetic step, and a relatively flat concentration profile is established within the film, consistent with the predictions of surface-limited Case II diffusion,[15] and consistent with our observation that the wrinkling amplitude of the target patterns did not change in the radial direction (Fig. 3d). In addition, Case II diffusion is characterized by a sharp interface between rubbery and glassy polymer at the solvent front[7] – this is expected to lead to a compressive stress in the film pushing outward along the perimeter of the diffusion front (Fig. 5c; see directional arrows in Fig. 5d). This stress field, combined with a probable decrease in lateral swelling and Poisson stresses due to the thicker crosslinked layer, results in the direction of maximum compressive stress being oriented in the radial direction. When this stress overcomes the critical wrinkling stress, the surface thus begins to wrinkle in concentric rings, producing target patterns.

To test the ability to control the formation location and morphology of spoke and target patterns, we performed two simple demonstrative experiments. For the spokes, we used a microsized spherical glass bead as a selective mask for UVO oxidation, to produce an

WILEY InterScience DISCOVER SOMETHING GREAT
© 2009 WILEY-VCH Verlag GmbH & Co. KGaA, Weinheim

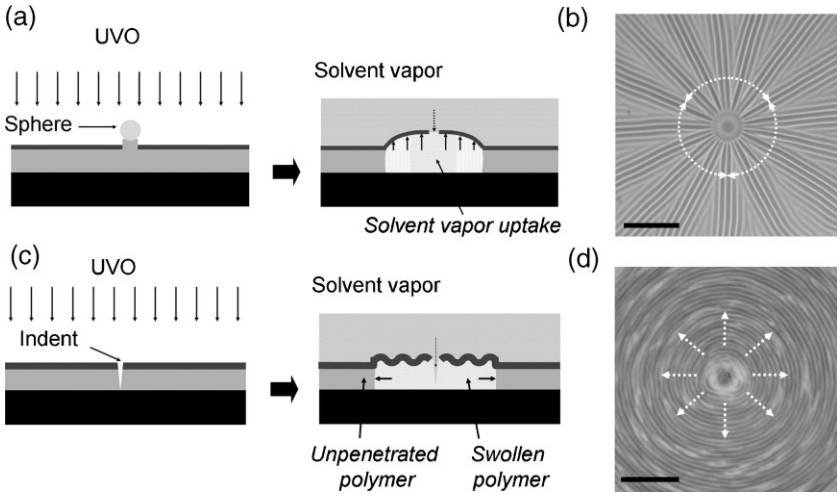

Figure 5. a) Schematics showing a possible mechanism for the emergence of spoke patterns. b) An optical microscopy image of the spoke pattern formed from a predefined unmodified region (≈15 μm in diameter) produced by selective masking with a microscale glass particle (30 μm to 50 μm in diameter) on a 700 nm thick PS film after $t_{UVO} = 3$ min. The image was taken after 150 s of toluene-vapor exposure. c) Schematics showing a possible mechanism for the emergence of target patterns. d) An optical microscopy image of the target pattern formed from a predefined point-like defect (≈5.6 μm in diameter) produced by indentation (Berkovich tip) on a 700 nm thick PS film after $t_{UVO} = 10$ min. The image was taken after 210 s of toluene-vapor exposure. The orientations of maximum in-plane compressive stress are schematically illustrated in b) and d), and the wrinkles are aligned orthogonal to the compressive stress axis. Scale bars = 30 μm.

unmodified region to act as a defect (Fig. 5a). After 3 min of UVO treatment, the center of defect was found to be at a higher elevation than its surroundings, because the defect prevents etching by UVO. On subsequent toluene vapor exposure, the PS-film surface wrinkled by localized swelling through this predefined defect. A topographic image of the wrinkled film showed a regular spokelike pattern around the round region of PS that was untreated, due to masking by the bead (Fig. 5b). On another film, we used a three-sided Berkovich-shaped diamond tip to indent a UVO-treated PS surface ($t_{UVO} = 10$ min; Fig. 5c). When the PS was exposed to toluene vapor, a pattern began to form at the indent site and spontaneously self-organized into concentric rings (Fig. 5d). Thus, with these experiments we were able to demonstrate the importance of localized defects to pattern initiation, as well as the dependence of pattern morphology on t_{UVO}. We note that the long-range order of patterns associated with single predefined defects was quite good – very regular patterns as large as a few millimeters in diameter were readily formed (Supporting Information, Fig. S1). In addition, these highly regular patterns could be further organized by predefining arrays of point-like or line defects (scratches) in the film prior to solvent exposure, demonstrating the rich variety of surface patterns and symmetries made possible by this technique (Supporting Information, Fig. S2).

The ability of the surface morphology to clearly and easily reflect not only the location of the solvent front, but also the type of diffusion kinetics, is remarkable. We anticipate that this system could be a useful experimental tool for diffusion-related research; for example, we expect that the Fickian diffusion behavior shown in the growth of the spoke patterns can be utilized to predict the diffusion coefficients (D) of solvents into polymers. Indeed, by taking the front growth in radial direction as the diffusion length, to a first approximation, as $R \approx (4Dt)^{1/2}$,[13] one can easily estimate D. From the experimental results given in Figure 4a, we obtain $D \approx 2.2 \times 10^{-7}$ cm^2 s^{-1} for the diffusivity of toluene into a PS film, which agrees well with previous reports in the literature ($D \approx 2.5 \times 10^{-7}$ cm^2 s^{-1}).[18] It is also worth emphasizing that the target-shaped concentric-ring patterns bear considerable visual resemblance to various types of patterns found, for example, in periodic precipitation (''Liesegang ring''), Turing instability, and droplet evaporation from a capillary bridge (''tears of wine'').[19] However, our target patterns exhibit distinctive characteristics both in the *spacing law* and *time law*, that is, $\lambda_{n+1}/\lambda_n = 1$ and $\lambda_n/t_n =$ constant, where λ_n and t_n are the spacing and formation time of the n-th ring, respectively. The spoke pattern somewhat resembles the capillary-driven wrinkling pattern recently reported,[20] but in this case λ increases with r. Our patterns appear to bear the closest resemblance to the structures observed recently by Chada and Yan in UV irradiated PS,[21] but they attributed their patterns to phase segregation of highly oxidized PS domains. Our hypothesis of diffusion-controlled wrinkling, which has been informed by kinetics studies and careful control of the ambient solvent concentration, appears to more fully explain the emergence of particular pattern morphologies and the rate of their growth. In addition, though we have focused on a PS–toluene system for the purposes of this study, our results are very general – examining other polymers and solvents, as well as changing parameters such as the film thickness, will allow for even greater control over the wavelength, morphology, and growth rate of the resulting patterns.

In conclusion, we have observed surface-wrinkling patterns on UVO-treated PS surfaces as a result of osmotically driven swelling associated with solvent-vapor sorption. The formation and growth kinetics of both spoke and target patterns originate from local defects in the crosslinked UVO-treated surface. Increasing t_{UVO} appears to limit the flux of solvent into the film at defect sites, resulting in a transition from Fickian to Case II diffusion behavior. The differences in diffusion kinetics establish different stress states in the film, leading to spoke and target patterns being associated with Fickian ($R \sim t^{1/2}$) and Case II ($R \sim t$) kinetics, respectively. This compelling evidence of the inherent connection between diffusion kinetics and pattern morphology will open up new directions for the field of instability-driven self-assembly and surface patterning.

Experimental

A 3% (by mass) solution of PS (atactic, $M_w = 654.4 \times 10^3$ g mol^{-1}; polydispersity index = 1.09; Polymer Source, Inc.) in toluene was spin-coated on a precleaned (UVO-treated for 5 min and rinsed with

© 2009 WILEY-VCH Verlag GmbH & Co. KGaA, Weinheim

toluene, and dried with nitrogen gas) silicon wafer at 1000 rpm for 60 s, providing a film thickness of several hundred nanometers as measured by reflectance interferometry (Model F20, Filmetrics). The sample was then exposed to UVO (Model 342, Jelight) for a controlled time at a distance of 1 cm from the UV lamp (lamp was first allowed to warm for at least 30 min). Tapping-mode AFM (Digital Instruments Dimension 3100 with a Nanoscope IV controller, Veeco Instruments) revealed no significant increase in surface roughness on samples with different UVO treatment times, consistent with previous literature [11]. The UVO-treated sample was then placed into a tightly sealed Pyrex chamber (volume $\approx$25 cm^3) containing toluene (volume $\approx$5 mL; anhydrous, 99.8%; Aldrich) at room temperature. The sample inside the sealed chamber was located at a distance of about 1 cm above the air/toluene-liquid interface, so that the sample was contacted by toluene vapor only. The developing wrinkling patterns on the surfaces of the polymer films were monitored in situ using optical microscopy (Labophot-2, Nikon Inc.) with a charge-coupled device (CCD) camera (Megaplus Model ES 1.0, Kodak). Tapping-mode AFM was performed on samples after removal from the chamber to characterize surface profile. Indentation with Berkovich and 1-μm 90° cone indenters (NanoIndenter XP, MTS System, Inc.) was used on the UVO-treated samples to produce well-defined defects.

Acknowledgements

The authors thank A. M. Forster for preparing microindented samples, H. W. Ro for helping with the X-ray reflectivity measurements, and J. F. Douglas for helpful discussion. A.J.N. gratefully acknowledges the NIST/NRC Postdoctoral Fellowship Program for funding. This work is an official contribution of the National Institute of Standards and Technology; not subject to copyright in the United States. Equipment and instruments or materials are identified in the paper in order to adequately specify the experimental details. Such identification does not imply recommendation by NIST, nor does it imply the materials are necessarily the best available for the purpose. The error bars presented throughout this manuscript represent one standard deviation of the data, which is taken as the experimental uncertainty of the measurement. Supporting Information is available online from Wiley InterScience or from the author.

Received: October 31, 2008
Revised: November 6, 2008
Published online: January 29, 2009

[1] a) N. Bowden, S. Brittain, A. G. Evans, J. W. Hutchinson, G. M. Whitesides, *Nature* **1998**, *393*, 146. b) C. M. Stafford, C. Harrison, K. L. Beers, A. Karim, E. J. Amis, M. R. Vanlandingham, H.-C. Kim, W. Volksen, R. D. Miller, E. E. Simonyi, *Nat. Mater.* **2004**, *3*, 545. c) P. J. Yoo, K. Y. Suh, H. Kang, H. H. Lee, *Phys. Rev. Lett.* **2004**, *93*, 034301. d) K. Efimenko, M. Rackaitis, E. Manias, A. Vaziri, L. Mahadevan, J. Genzer, *Nat. Mater.* **2005**, *4*, 293. e) M. W. Moon, S. H. Lee, J. Y. Sun, K. H. Oh, A. Vaziri, J. W. Hutchinson, *Proc. Natl. Acad. Sci. USA* **2007**, *104*, 1130.

[2] a) N. Bowden, W. T. S. Huck, K. E. Paul, G. M. Whitesides, *Appl. Phys. Lett.* **1999**, *75*, 2557. b) D. B. H. Chua, H. T. Ng, S. F. Y. Li, *Appl. Phys. Lett.* **2000**, *76*, 721.

[3] E. Cerda, L. Mahadevan, *Phys. Rev. Lett.* **2003**, *90*, 074302.

[4] J. Genzer, J. Groenewold, *Soft Matter* **2006**, *2*, 310.

[5] E. P. Chan, A. J. Crosby, *Soft Matter* **2006**, *2*, 324.

[6] a) V. Fleury, J. H. Kaufman, D. B. Hibbert, *Nature* **1994**, *367*, 345. b) M. Assenheimer, V. Steinberg, *Nature* **1994**, *367*, 435. c) T. Hayashi, R. W. Carthew, *Nature* **2004**, *431*, 647. d) L. Gránásy, T. Pusztai, G. Tegze, J. A. Warren, J. F. Douglas, *Phys. Rev. E* **2005**, *72*, 011605. e) M. K. Chaudhury, J. Y. Chung, *Langmuir* **2007**, *23*, 8061.

[7] a) N. L. Thomas, A. H. Windle, *Polymer* **1982**, *23*, 529. b) T. P. Gail, E. J. Kramer, *Polymer* **1991**, *32*, 265.

[8] R. E. Johnson, R. H. Dettre, *J. Phys. Chem.* **1964**, *68*, 1744.

[9] J. Y. Chung, J. P. Youngblood, C. M. Stafford, *Soft Matter* **2007**, *3*, 1163.

[10] a) J. Y. Chung, M. K. Chaudhury, *J. R. Soc. Interface* **2005**, *2*, 55. b) E. P. Chan, E. J. Smith, R. C. Hayward, A. J. Crosby, *Adv. Mater.* **2008**, *20*, 711.

[11] a) D. O. H. Teare, C. Ton-That, R. H. Bradley, *Surf. Interface Anal.* **2000**, *29*, 276. b) D. O. H. Teare, N. Emmison, C. Ton-That, R. H. Bradley, *Langmuir* **2000**, *16*, 2818.

[12] a) E. Bonaccurso, H.-J. Butt, K. Graf, *Eur. Polym. J.* **2004**, *40*, 975. b) K. Büscher, R. Berger, W. Brünger, K. Graf, *Microelectron. Eng.* **2006**, *83*, 819.

[13] W. M. Deen, *Analysis of Transport Phenomena*, Oxford University Press, New York **1998**, p. 91.

[14] H. Vandeparre, P. Damman, *Phys. Rev. Lett.* **2008**, *101*, 124301.

[15] P. J. McDonald, J. Godward, R. Sackin, R. P. Sear, *Macromolecules* **2001**, *34*, 1048.

[16] V. Reichert, S. K. Basu, L. F. Francis, A. V. McCormick, L. E. Scriven, *Prog. Org. Coat.* **2008**, *63*, 33.

[17] H. Q. Jiang, D. Y. Khang, J. Z. Song, Y. G. Sun, Y. G. Huang, J. A. Rogers, *Proc. Natl. Acad. Sci. USA* **2007**, *104*, 15607.

[18] a) E. Bonaccurso, H. J. Butt, B. Hankeln, B. Niesenhaus, K. Graf, *Appl. Phys. Lett.* **2005**, *86*, 124101. b) J. Rauch, W. Köhler, *Phys. Rev. Lett.* **2002**, *88*, 185901.

[19] a) B. A. Grzybowski, K. J. M. Bishop, C. J. Campbell, M. Fialkowski, S. K. Smoukov, *Soft Matter* **2005**, *1*, 114. b) Z. Lin, S. Granick, *J. Am. Chem. Soc.* **2005**, *127*, 2816.

[20] J. Huang, M. Juszkiewicz, W. H. de Jeu, E. Cerda, T. Emrick, N. Menon, T. P. Russell, *Science* **2007**, *317*, 650.

[21] S. Chada, M. Yan, *Soft Matter* **2008**, *4*, 2164.

WILEY InterScience® DISCOVER SOMETHING GREAT

© 2009 WILEY-VCH Verlag GmbH & Co. KGaA, Weinheim